Recent advances in mathematical modeling and statistical analysis of exocytosis in endocrine cells

Morten Gram Pedersen[a,*], Alessia Tagliavini[a],
Giuliana Cortese[b], Michela Riz[a,c], Francesco Montefusco[a]

[a]*Department of Information Engineering, University of Padua,
Via Gradenigo 6/B, 35131 Padova, Italy*
[b]*Department of Statistical Sciences, University of Padua,
Via Cesare Battisti 141, 35121 Padova, Italy*
[c]*Sanofi, Industriepark Höchst, 65926 Frankfurt am Main, Germany*

Abstract

Most endocrine cells secrete hormones as a result of Ca^{2+}-regulated exocytosis, i.e., fusion of the membranes of hormone-containing secretory granules with the cell membrane, which allows the hormone molecules to escape to the extracellular space. As in neurons, electrical activity and cell depolarization open voltage-sensitive Ca^{2+} channels, and the resulting Ca^{2+} influx elevate the intracellular Ca^{2+} concentration, which in turn causes exocytosis. Whereas the main molecular components involved in exocytosis are increasingly well understood, quantitative understanding of the dynamical aspects of exocytosis is still lacking. Due to the nontrivial spatiotemporal Ca^{2+} dynamics, which depends on the particular pattern of electrical activity as well as Ca^{2+} channel kinetics, exocytosis is dependent on the spatial arrangement of Ca^{2+} channels and secretory granules. For example, the creation of local Ca^{2+} microdomains, where the Ca^{2+} concentration reaches tens of μM, are believed to be important for triggering exocytosis. Spatiotemporal simulations of buffered Ca^{2+} diffusion have provided important insight into the interplay between electrical activity, Ca^{2+} channel kinetics, and the location of granules and Ca^{2+} channels. By confronting simulations with statistical time-to-event (or survival) regression analysis of single granule exocytosis monitored with TIRF microscopy, a direct connection between location and rate of exocytosis can be obtained at the local, single-granule level. To get insight into whole-cell secretion, simplifications of the full spatiotemporal dynamics have shown to be highly helpful. Here, we provide an overview of recent approaches and results for quantitative analysis of Ca^{2+} regulated exocytosis of hormone-containing granules.

Keywords: Hormone secretion, Ca^{2+} microdomains, Spatiotemporal Ca^{2+} dynamics, Mixed-effects modeling, Survival analysis, α-cells, β-cells, Pituitary

---

[*]Corresponding author
Email address: `pedersen@dei.unipd.it` (Morten Gram Pedersen)

cells, Secretory granules, Large dense-core vesicles

---

1. Introduction

The endocrine system is a physiologically important collection of glands that secrete different kind of hormones to control other target cells [1]. Prototype endocrine cells include the pancreatic α- and β-cells, andrenal chromaffin cells, and pituitary cells. Their crucial role in regulating various physiological processes makes the study of the cellular mechanisms in endocrine secretory cells of great importance. In particular, functional impairment of these cells leads to serious diseases such as diabetes [2].

In most endocrine cells, the hormones are contained in secretory granules that, in response to a series of cellular mechanisms culminating with an increase in the intracellular Ca^{2+} concentration, fuse with the cell membrane, a process denoted exocytosis. The main events underlying hormone exocytosis and release are shared with exocytosis of synaptic vesicles underlying neurotransmitter release in neurons [3, 4].

The molecular machinery involved in exocytosis is increasingly well understood, and involves isoforms of the SNARE proteins syntaxin and and SNAP, which are located in the cell membrane, and VAMP, also called synaptobrevin, inserted into the vesicle/granule membrane [4]. The SNARE proteins can form a so-called SNARE complex, which drives fusion of the two membranes, which – in the case of endocrine cells – allows the hormone molecules contained in the granule to exit the granule and enter the blood stream. SNARE complexes interact with many other proteins, notably Ca^{2+}-sensing proteins such as synaptotagmins, which trigger exocytosis upon Ca^{2+} binding [4]. Thus, the local Ca^{2+} concentration at the Ca^{2+} sensor of the exocytotic machinery is an important determinant of the probability (rate) of exocytosis of the secretory granule. This fact will be a recurrent theme in the present paper.

Depending on their ability to undergo exocytosis, granules in endocrine cells are frequently divided functionally into a readily releasable pool (RRP) and a number of reserve pools [5–9]. The readily releasable granules are immediately available for secretion and typically consists of 1%-5% of the total number of granules in the cell [7]. After exocytosis of these granules, the RRP is resupplied by granules from the reserve pools. However it is still unclear if the refilling process involves physical translocation of granules within the cell, chemical modification of granules already situated at the membrane, recruitment of exocytotic proteins, or a combination of these processes, which are commonly referred to as priming [10–12]. In this paper we will not review mathematical models of the dynamics of the granule pools, but focus only on quantitative approaches to the study in the last step in the life of a secretory granule, i.e., exocytosis (see e.g. [13, 14] for recent reviews of models of granule pools in β-cells, and [9] for a discussion of pools and models of synaptic vesicles).

2. Experimental techniques for investigations of exocytosis

2.1. Recording single exocytotic events

Using the patch-clamp technique, individual exocytotic events occurring in a patch of the cell membrane can be observed at discrete steps in membrane capacitance C_m [15–18]. For instance, the fusion of a 300-nm-diameter granule with the plasma membrane yields an electrically detectable step in C_m of 2-3 fF [1, 7]. However, the observation of such events is somewhat "lucky punches" in the sense that it is impossible beforehand to estimate the number of granules in the investigated membrane patch, and thus, the experimenter has little idea of the maximal or expected number of exocytotic events that can be observed in response to a stimulus. Hence, rates of exocytosis of the single granules (i.e., the number of events divided by the total number of available granules) can not be estimated reliably from such data.

Live-cell imaging provides an alternative experimental method for the study of single exocytotic events. For example, two-photon imaging of pancreatic islets bathed in the tracer sulforhodamine-B allows the detection of single fusion events as the tracer enters the granule through the fusion pore, resulting in bright spots below the cell membrane [19–21]. A major advantage of this technique, due to the two-photon microscopy technique is the possibility to monitor exocytosis in cells deep within their natural environment, i.e., within intact pancreatic islets, whereas e.g. capacitance recordings typically are performed on single cells or membrane patches. However, the use of sulforhodamine-B as an extracellular marker does not allow the visualization of secretory granules before they undergo exocytosis. Thus, as for the electrophysiological methods, the single-granule rate of exocytosis can not be estimated.

In contrast, labeling of the secretory granules with one of several fluorescent markers [22, 23] allows the experimenter to follow the single granules with the use of total internal reflection fluorescence (TIRF) microscopy [11, 24–31]. TIRF imaging excites fluorescent reporters in a thin (a few hundred nanometer) layer below the cell membrane attached to the coverslip, thus allowing observation of the granules located at the membrane while minimizing the signal from granules deeper within the cells. It is therefore possible to investigate three-dimensional spatial movement of the granules as they approach the membrane, become ready for exocytosis, and eventually undergo exocytosis. Combined with other fluorophores and two-color imaging, it is possible to monitor e.g. Ca^{2+} levels [32, 33] or protein abundance [11, 29, 34] at the individual granules. With such data it is possible to relate rates of exocytosis to signals and molecules controlling single fusion events. An example of such an analysis is given below (Section 4).

2.2. Measuring whole-cell exocytosis as capacitance increases

Monitoring the total cellular amount of exocytosis in response to various stimuli can relatively easy be performed using the patch-clamp technique. As mentioned above, the fusion of granules with the plasma membrane effectively increases the area of the cell membrane. Since the membrane capacitance is proportional to the area, this leads to an increase in whole-cell capacitance, which

3

can be measured using either the whole-cell or the perforated-patch variants of patch-clamping [1, 7, 35].

Two major stimulation protocols have been applied to investigate rapid exocytosis in various endocrine cells. One option, which is typically used to investigate directly the Ca^{2+} sensitivity of the exocytotic machinery, is to load the cell via the patch pipette with "caged" Ca^{2+}, i.e., Ca^{2+} bound to a light-sensitive buffer, which upon light stimulation is released [1, 3]. This so-called "flash release" rapidly increases the Ca^{2+} concentration uniformly in the cell to levels that can be measured simultaneously which Ca^{2+} sensitive probes. By relating the Ca^{2+} levels to the increases in membrane capacitance as a measure of exocytosis, it has been revealed that endocrine exocytosis typically occurs when the Ca^{2+} concentration is raised to tens of μM [36–38]. More recently, pools with higher Ca^{2+} sensitivity ($\sim 2\ \mu M$) were found in chromaffin [39] and β-cells [40, 41]. In chromaffin cells, the capacitance traces can typically be described as a sum of exponentials, which led to a mathematical model describing the exocytotic response as occurring from two different pools that are mutually connected [6]. Recently, this model was simplified by assuming that a priming step was Ca^{2+} dependent, and by confronting the models with experimental data, the authors concluded that the sequential model with release from a single pool effectively described Ca^{2+}-dependent properties of secretion [42].

Although flash-release gives important insight into the Ca^{2+}-sensitivity of the release machinery, the method is unphysiological since Ca^{2+} is raised artificially, and not because of Ca^{2+} influx via voltage-dependent Ca^{2+} channels [3]. A more physiological protocol is to depolarize the cell, which opens Ca^{2+} channels, and consequently triggers Ca^{2+} influx and exocytosis [1, 3]. During the depolarization it is possible to measure the Ca^{2+} current, whereas the cell capacitance can only be measured reliably before and after, but not during, the depolarization. To investigate the kinetics of exocytosis it is therefore necessary to apply depolarizing pulses of varying duration. The analysis of this so-called pulse-length protocol was recently performed in details [13] as summarized in Section 6.1.

2.3. Clustered data

Although not uniquely related to the investigations of exocytosis, we wish for a moment to dwell upon the statistical analysis of cell biological experiments. Typically, several observations are performed in the same cell, e.g., subsequent depolarizations to evoke exocytosis, or imaging recordings of many exocytotic events within the same cell. Such experimental data have an inherent clustered structure where observations performed on the same cell correspond to a cluster. It should be expected that measurements from the same individual cell are correlated since they share some specific characteristics of that cell. For example, some cells may be highly-responding, while others are not, and hence, if e.g. a large amount of exocytosis is measured in response to a first depolarization, it should be expected that a subsequent depolarization also triggers much exocytosis. Therefore, it seems reasonable to assume that the recordings from a single cell are independent between each other only if we condition on

4

the cluster, while observations in different cells are independent (independence between clusters).

If the data analysis is performed on pooled data, i.e., neglecting the fact that the data was obtained from different cells that have natural cell-to-cell heterogeneity, inference may be distorted, although maximum likelihood estimates obtained ignoring clustering are valid. It is a well-known fact in the statistical literature [43, 44], but often not considered in biology, that ignoring clustering typically leads to underestimation of standard errors, and thus to small 'naive' p-values.

A commonly used approach to correct for clustering is to estimate the variance-covariance matrix using the so-called *robust* or *sandwich* estimator $\mathcal{R}$ [44]. From $\mathcal{R}$, robust standard errors for maximum likelihood estimates (obtained neglecting clustering), and correct Wald-type 95% confidence intervals can be obtained. More advanced likelihood methods based on the sandwich estimator have also been proposed [44].

Mixed-effects models [13, 45] provide an alternative statistical approach to take into account natural cell heterogeneity, and to handle the situation with intra-cellular correlation and random variation due to biological differences between cells. In these models, fixed effects that describe the main interest of the study, e.g., difference between groups, are combined with random effects that model how the individual cell responses deviate from the group average. Thus, in contrast to the adjustments based on the sandwich estimator, the cell-to-cell variation is modeled, which allows the investigator to quantify cell heterogeneity, while providing correct estimates of standard errors of the fixed effect parameters.

Finally, a more extreme way to remove the clustering problem is to average measurements from one cell into a single data point. Although this approach takes care of the clustering problem, it discards information in the data, which reduces the power of the statistical tests considerably, and may bias the final result. Further, for some experiments, such as the pulse-length depolarization protocol (see Section 6.1), data from one cell cannot be summarized to a single data point in a straightforward, meaningful way. The statistical approaches mentioned above use all information in the data, but adjust, e.g., standard errors and p-values for the presence of clustering.

3. Local control of exocytosis by Ca^{2+} microdomains

Mathematical modeling has played an important role for the development of current theories of the control of neurotransmitter and hormone release. Whereas it was early well-established that Ca^{2+} influx is crucial for triggering exocytosis in neurons [46] and endocrine cells [47, 48], the spatial organization of the Ca^{2+} channels and the release machinery is only beginning to be clarified (see e.g. [49] and Section 4). Thus, for decades mathematical modeling was the main approach to study the relation between individual granules and single Ca^{2+} channels.

5

Chad & Eckert [50] and Simon & Llinas [51] presented important simulation studies of the spatiotemporal Ca^{2+} profiles below and around open Ca^{2+} channels, reaching similar conclusions. Their main results were that local Ca^{2+} *microdomains* build up in microseconds below open Ca^{2+} channels, and collapse just as rapidly when the channels close. When a Ca^{2+} channel is open, the local Ca^{2+} concentration reaches tens to hundreds of μM, which decays within tens of nm from the channel. Based on these simulation results it was proposed that the spatial localization of the synaptic vesicles compared to the Ca^{2+} channels is of great importance for determining the amount of neurotransmitter release, since vesicles near the channels will be exposed to much higher Ca^{2+} concentrations. Consequently, the relation between synaptic release and the whole-cell Ca^{2+} current, which is given as the product of the number of open Ca^{2+} channels and the single channel current, becomes less intuitive. Whereas the number of open channels increases when the membrane potential becomes depolarized, the Ca^{2+} driving force and hence the single channel current decreases. This means that there will be more Ca^{2+} microdomains in response to depolarizations, but each microdomain will have lower Ca^{2+} concentration. This will be discussed in greater details below (Section 6). We refer to Neher [52, 53] for classical reviews of Ca^{2+} microdomains and related modelling.

Whereas these earlier studies of microdomain dynamics explained well aspects of neurotransmitter release such as the speed of synaptic signalling after arrival of an action potential, and the rapid cessation of release following repolarization because of the collapse of the microdomains, it later became clear that the slower release from endocrine cells might not be explained by pure microdomain release. Klingauf & Neher [54] modelled diffusion around Ca^{2+} channels in adrenaline-secreting chromaffin cells paying particular attention to the choice of buffer parameters. By coupling the simulated Ca^{2+} profiles to a model of exocytosis developed from experiments involving flash-released Ca^{2+}, they could simulate exocytosis under various conditions, which was then compared to experimental results. They found that release from chromaffin cells is well-described by an arrangement where the Ca^{2+} sensors of most granules are located ~ 300 nm from Ca^{2+} channels, while the exocytotic machinery of a small ($\sim 8\%$) pool of granules is located at ~ 30 nm from the channels [54]. Since the major part of the granules are located some distance from Ca^{2+} channels, buffering parameters become important for the control of Ca^{2+} levels and exocytosis. In summary, these authors proposed that in (neuro-)endocrine cells most exocytosis occurs outside microdomains.

The roles of Ca^{2+} buffering and diffusion obstacles were further studied by diffusion modeling in pituitary cells [55], and with Monte Carlo simulations in neurons [56]. These studies found that diffusion barriers, such as intracellular structures [55], or the synaptic vesicles themselves [56], can profoundly modify the spatiotemporal Ca^{2+} profiles which might influence the amount of exocytosis, partly because of Ca^{2+} buffer saturation [55]. Further, electrostatic forces may influence the formation and shape of microdomains [57]. The interactions and relative importance of these and other local effects on Ca^{2+} microdomains and exocytosis are still to be clarified, both experimentally as well as theoreti-

6

cally.

4. Mathematical and statistical modeling of local Ca^{2+} control of exocytosis in β-cells

Insulin is released from pancreatic β-cells in response to elevated glucose levels, and disturbed insulin secretion is now generally recognized as pivotal for the development of diabetes [2]. The hormone acts on target tissues such as the liver, muscles and fat cells to reduce glucose production and promote glucose uptake.

We have recently been involved in a study investigating how local Ca^{2+} relates to exocytosis of insulin-containing granules (Gandasi et al., *submitted*). Using TIRF microscopy, labelled granules and Ca^{2+} levels were monitored simultaneously in insulin-secreting β-cells. A major question of interest is the spatial organization of the secretory granules and the Ca^{2+} channels that provide the influx of Ca^{2+}, which triggers exocytosis.

We performed spatiotemporal simulations of buffered Ca^{2+} diffusion using the simulation software CalC [58] in order to investigate how distance to the nearest Ca^{2+} channels was related to the Ca^{2+} level at the secretory granule (Fig. 1). Because of the nonlinear properties of the fluorescent Ca^{2+} sensor and cell-to-cell variance, we found that the absolute value of the fluorescent signal was a poor proxy for this distance. In contrast, the risetime of the Ca^{2+} sensor signal was a much more robust readout of how far the granule was located from a Ca^{2+} channel. The risetime of the Ca^{2+} signal was found to be proportional to the square of the distance to the channel, as can be expected for a diffusion process. In this way, we estimated the distance to the nearest Ca^{2+} channel for each single granule, and histograms of the distances for granules that underwent exocytosis (responders) could be compared to non-responders. As expected, non-responders were located further away from Ca^{2+} channels. However there was a large overlap between the two distributions, suggesting that exocytosis also occurs at some distance from Ca^{2+} channels and not only from microdomains. Using electrophysiological techniques, we reached a similar conclusion in another study [59]. This also corresponds to the conclusions in the modeling study by Klingauf & Neher [54].

We moved on to investigate directly how the risetime of the Ca^{2+} sensor signal (as a proxy for distance to a Ca^{2+} channel) at the individual granules was related to their rate of exocytosis using time-to-event analysis (Gandasi et al., *submitted*). Time-to-event (also known as survival or failure time) analysis is an area of statistics typically used for clinical or demographic data where individuals are followed over time until either the observation of a certain event of interest, such as death, onset of disease, conception, first-time marijuana use, etc., or until they exit the study with no event or the end of the study [60, 61]. Another common area of its application is reliability engineering where the interest is the time to failure of an instrument or machine [62]. The data structure in such contexts of application is similar to the TIRF exocytosis data, which
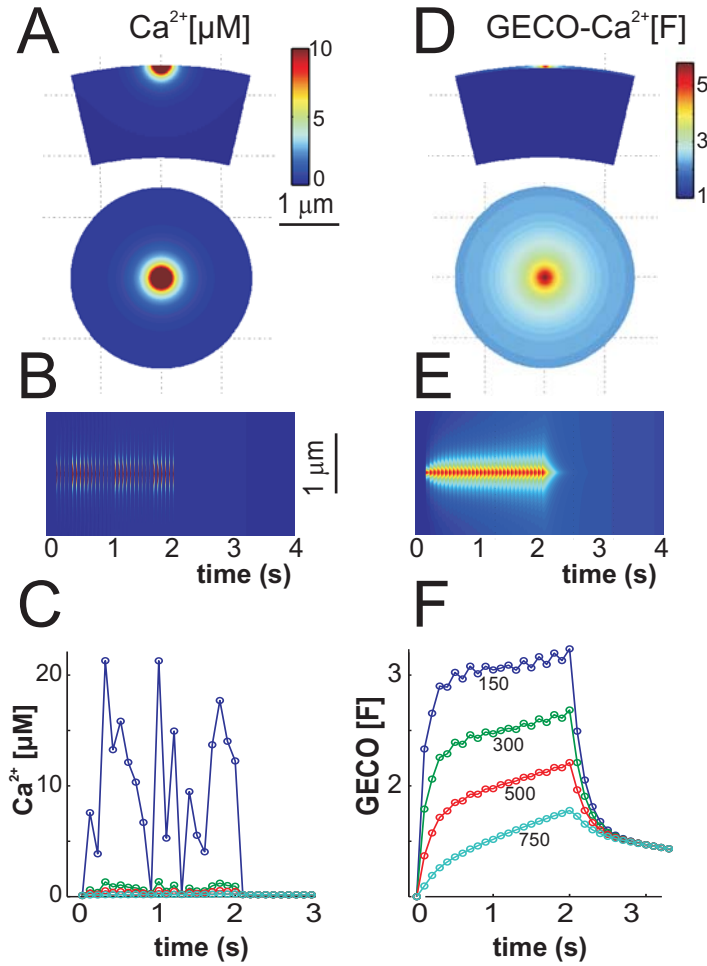
Figure 1: A) Simulation of $[Ca^{2+}]$ as function of the distance from three open Ca^{2+}-channels, viewed as section through the cell (upper) or facing the cell (lower). B) Evolution of $[Ca^{2+}]$ over time and distance along the plasma membrane. C) Average $[Ca^{2+}]$ over time in a circle centered at the channel cluster with radius 150 nm (blue), or consecutive annuli with outer radius of 300 nm (green), 500 nm (red), 750 nm (light blue). D-F) as in panels A-C, but convolved with the parameters of the imaging system and the Ca^{2+} sensor. Note that because of saturation of the Ca^{2+} sensor, in panel F the amplitudes are more similar than in panel C, but differences in risetime remain.

allowed us to apply these well-established statistical methods on completely different biological and temporal scales.

Risetime was measured as the time it took for the Ca^{2+} sensor signal at each granule to reach its half maximum ($t_{1/2}$). To quantify how the risetime influences the rate of exocytosis, we fitted Cox's proportional hazards regression models with $\log(t_{1/2})$ as covariate. To account for cell-to-cell variation, granules within a cell were considered as clustered data (Section 2.3) and a marginal Cox model was used to obtain robust estimates of standard errors [61]. We found that the rate of exocytosis drops by ∼50% when the risetime doubles. Using the quadratic relation between distance and risetime, obtained from diffusion modeling as explained above, allowed us to go from distance to risetime, and with the results from the Cox regression model, to the rate of exocytosis. Accordingly, we estimated that if a Ca^{2+}-channel moves 50% closer to a granule the release probability increases approximately four fold. In summary, this study (Gandasi et al., *submitted*) shows how the combination of advanced statistical modeling and state-of-the-art spatiotemporal mathematical simulations enables quantification of the control of single-granule exocytosis.

In another work (Cortese et al., *submitted*), we applied time-to-event analysis to exocytosis data from healthy and diabetic human β-cells monitored with TIRF microscopy to quantify rates of exocytosis and pool sizes. In survival analysis, univariate frailty modeling is a method to take into account unobserved differences in rates between individuals [63]. Since TIRF imaging of the secretory granules can not reveal their release propensity, i.e., whether they belong to the immediately releasable pool (IRP) of granules, we allowed for unobserved heterogeneity by including frailties in our statistical model. This approach allowed us to estimate the size of the IRP directly from single-granule exocytosis data, which we found to be ∼2.6% of the docked granules, i.e. ∼20 granules per human β-cell, in healthy individuals, whereas the IRP was about half as big in diabetic β-cells.

We thus conclude that time-to-event analysis methods can be advantageously applied to cell biological data to provide statistically sound results on completely different biological and temporal scales than their typical areas of application, as showed by the two studies mentioned here.

5. How do different pattern of electrical activity relate to local control of exocytosis?

Endocrine pituitary cells (i.e., melanotrophs, lactotrophs, somatotrophs, thyrotrophs, corticotrophs, and gonatotrophs) secrete a wide number of hormones in response to stimuli from the hypothalamus. The pituitary hormones act on other endocrine cells and other tissues including the brain to regulate physiological and behavioral aspects of growth, metabolism, water balance, and reproduction [1]. The pituitary cells express different ion channels and are electrically excitable. In particular, electrical activity induces an intracellular Ca^{2+} elevation causing hormone secretion. The two typical electrical patters

observed in these cells are continuous spiking – typically observed in luteinizing hormone-secreting gonadotrophs under basal conditions – and a form of bursting known as pseudo-plateau bursting often observed in prolactin-secreting lactotrophs, growth hormone-releasing somatotrophs, and ACTH-secreting corticotrophs, where the burst duration is at most a few seconds and the spikes that ride on the elevated voltage plateau are very small [64]. Various studies has highlighted an important role for large-conductance Ca^{2+}-sensitive K^+ (BK) channels in promoting bursting in pituitary cells [65, 66]. Simultaneous measurements of both electrical activity and Ca^{2+} concentration have established that the amplitude of Ca^{2+} fluctuations is greater in a bursting cell than in a spiking cell [65], leading to the hypothesis that bursting cells release more hormones than spiking cells [64]. Simultaneous single-cell measurements of electrical activity, Ca^{2+} and release should be performed in order to test this hypothesis experimentally, however this is not yet technically feasible.

Recently, we exploited a hybrid experimental/modeling approach to explore the hypothesis that bursting cells release more hormone than spiking cells [67]. We built a mathematical model of stochastic Ca^{2+} channel activity, Ca^{2+} diffusion and binding to buffer, and finally Ca^{2+}-driven exocytosis. The model was driven by experimentally recorded voltage traces exhibiting spiking and bursting patterns in the same cell (Fig. 2). The shift from one type of electrical activity to the other was obtained using either BK channels blockers or the dynamic clamp technique, which injects an artificial BK-current into the cell [66, 67].

We simulated realistic, stochastic Ca^{2+} channel kinetics in response to the recorded electrical traces. The resulting stochastic Ca^{2+} influx was then used to simulate buffered Ca^{2+} diffusion using CalC [58]. We then located the exocytosis machinery at different distances from the Ca^{2+} channel and used the Ca^{2+} concentration at that location to drive the exocytosis model (Fig. 2). This allowed us to calculate the average number of fused granules over time at different distances, and as a function of the total Ca^{2+} charge entry. First, we assumed the presence of a primed pool of granules [67]. We observed that when the release site was located 100 nm from the channel, exocytosis would be similar with both spiking and bursting, since the Ca^{2+} concentrations at the exocytotic machinery are in both cases saturating, and hence the primed pool is released at maximum speed within a few seconds whether driven by spiking or bursting electrical activity. Bursting triggered more exocytosis than spiking when the release site was situated further from the channel, at 300 nm or 500 nm, but in either case the primed pool was depleted fairly rapidly [67].

Most secretion measurements are made from a cell population over a period of minutes or tens of minutes. In such measurements the resupply of the primed pool by the reserve granule pool is rate limiting. We therefore simulated the effects of resupply by emptying the primed pool at the beginning of the simulation [67].

In this case, bursting evokes more release regardless of the distance between the channel and the granule. This is in spite of the fact that at short distances the local Ca^{2+} concentration saturates the release site, and highlights the importance of the dependence of resupply on the global, rather than local, Ca^{2+}
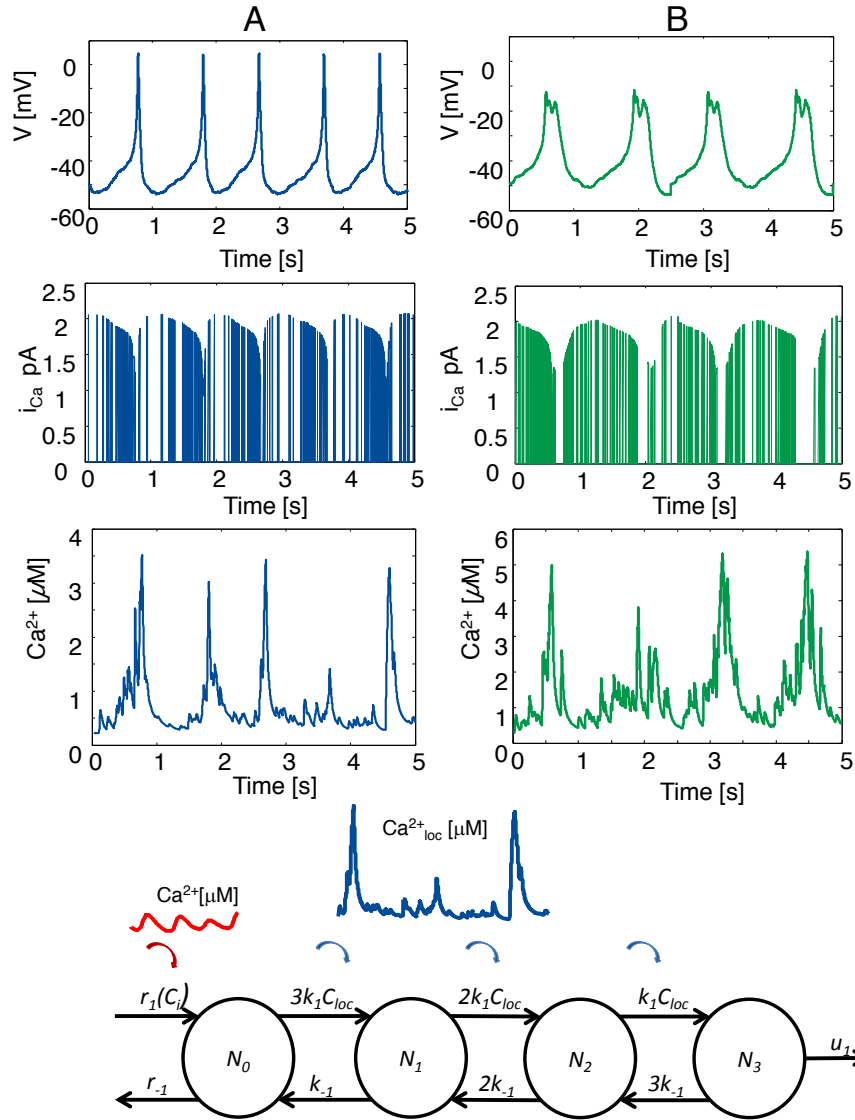
10

Figure 2: An overview of the hybrid experimental-modeling approach [67]. Recorded spiking (A) or bursting (B) electrical activity (upper row) was used to calculate stochastic single channel currents i_{Ca} (second row), which were used to simulate $[Ca^{2+}]$ at different distances from the channels (third row). The Ca^{2+} traces at different distances were then fed into a model of exocytosis to calculate secretion (lower).

concentration in our model. That is, the simulated global Ca^{2+} concentration is higher during bursting than during spiking, and this results in a greater rate of resupply in response to bursting. When the channel is close to the release site all granules becoming available due to the resupply are fused almost immediately, so resupply is rate limiting. Farther than 200 nm from the channel, local Ca^{2+} concentrations start to play a predominant role since the exocytosis machinery is no longer saturated, and therefore differences in local Ca^{2+} levels as well as global levels are responsible for differences in the exocytosis rates.

There are two factors that contribute to the greater effectiveness of bursting at evoking secretion in the model. One is that bursting brings in more Ca^{2+}, which increases the resupply rate relative to spiking, as mentioned above. The other is that the dynamics of Ca^{2+} diffusion and the exocytotic machinery favor the bursting signal over the spiking signal. That is, bursting is more efficient than spiking at evoking release. To test the latter, we plotted the number of fused granules versus the total Ca^{2+} entry Q. For release sites closer than 200 nm from the channel the efficiency of the spiking and bursting patterns were virtually the same. It is only at distances of 200 nm or greater that bursting becomes more efficient than spiking, since at these distances the number of fused granules per total Ca^{2+} entry is larger when the cell is bursting. This is due to the longer duration of the bursting events, which produce longer-duration Ca^{2+} signals that are advantageous for the exocytosis machinery that requires the binding of three Ca^{2+} ions to evoke granule fusion. In fact, in simulations in which only two Ca^{2+} ions are needed to evoke fusion, the efficiency of spiking and bursting are the same at a 200 nm distance, and bursting is only slightly more efficient at 300 and 500 nm distances.

Interestingly, at increased spike frequency, our model suggested that bursting was no longer superior to spiking when normalizing to Ca^{2+} influx. This is because the interval between each increase in local Ca^{2+} shortens, so the higher effectiveness of bursting might only be observed for release sites further away from the channels. Nevertheless, the bursting pattern caused by the presence of a BK current evoked more granule fusion because of the high average bulk Ca^{2+} during bursting, which results in higher rate of replenishment of the primed granules. If spiking frequency is further increased relative to bursting frequency so that the total amount of active time is the same, then bulk Ca^{2+} will be similar and so will the priming rate. In that sense, the bursting pattern is not more effective than the spiking pattern if the amount of activity (and therefore Ca^{2+} entry) is normalized.

In summary, we found that bursting is typically more effective at evoking secretion than is continuous spiking [67]. When bursting is induced in a spiking gonadotroph by injecting a BK-type current with dynamic clamp, the burst pattern is generally at least as effective as continuous spiking at evoking hormone release, and is often considerably more effective. The superiority of bursting over spiking is due to the fact that bursting brings more Ca^{2+} into the cell, thus augmenting both local and global Ca^{2+} levels, which in turn increases re-supply of secretory granules and exocytosis. However, we further observed that when spiking frequency is higher, this difference between spiking and bursting

12

in evoking exocytosis is considerably reduced.

6. From local to global: whole-cell modeling of exocytosis

Whole-cell imaging of Ca^{2+} has become a routine experiment, and many mathematical models of global Ca^{2+} levels have been published, also for endocrine cells. However, as discussed in the previous sections, local Ca^{2+} levels near Ca^{2+} channels determine the rate of exocytosis of the granules. Whole-cell Ca^{2+} levels reflect microdomain Ca^{2+} concentrations as well as the number of such microdomains in a rather simple way, as can be seen as follows.

The prototype model of the bulk cytosolic Ca^{2+} concentration, Ca_c, neglecting internal stores, is

$$\frac{d\,Ca_c}{dt} = f(-\alpha I_{Ca} - k\,Ca_c), \tag{1}$$

where f is the ratio of free (non-buffered) to total Ca^{2+}, α changes current to flux, and k is the rate parameter for Ca^{2+} extrusion. The whole-cell Ca^{2+} current is typically modeled in a Hodgkin-Huxley fashion as

$$I_{Ca} = g_{Ca}m^n h\,(V - V_{Ca}) \quad , \quad g_{Ca} = n_{Ca}\gamma, \tag{2}$$

with m and h activation and inactivation variables, respectively, and Ca^{2+} Nernst potential V_{Ca}. The maximal whole-cell conductance g_{Ca} is given as the product of the number of Ca^{2+} channels, n_{Ca}, and the single-channel conductance γ.

From Eq. 1, we obtain that at steady-state,

$$Ca_c = -\alpha I_{Ca}/k = -\alpha/k \left[n_{Ca}m^n h\right]\left[\gamma(V - V_{Ca})\right]. \tag{3}$$

Thus, the bulk Ca^{2+} level is proportional to the number of open channels, $n_{Ca}m^n h$, and to the single-channel current $i_{Ca} = \gamma(V - V_{Ca})$. Assuming a discrete spatial distribution of the Ca^{2+} channels, the number of microdomains is also equal to $n_{Ca}m^n h$. Further, the local Ca^{2+} concentration is proportional to i_{Ca} [52]. Thus, under moderate assumptions, the bulk cytosolic Ca^{2+} concentration is proportional to both the number of microdomains and to the microdomain Ca^{2+} concentration Ca_{md}, and hence also to the average microdomain Ca^{2+} levels $\overline{Ca}_{md}$, i.e., the average of local Ca^{2+} levels near the Ca^{2+} channels, whether open or closed,

$$Ca_c \propto \overline{Ca}_{md} = m^n h\,Ca_{md}. \tag{4}$$

During electrical activity or voltage-clamp depolarizations, Ca^{2+} enters the cell via Ca^{2+} channels, and exocytosis is controlled by the non-uniform Ca^{2+} concentrations around Ca^{2+} channels and in the submembrane space. Nonetheless, a common, but (as will be discussed in details below) erroneous, way of modeling exocytosis during such conditions, is to let whole-cell exocytosis be a (typically) nonlinear function of Ca_c. However, this approach is valid for the

study of exocytosis in response to flash-released buffered Ca^{2+}, which elevates the Ca^{2+} concentration uniformly. Under this experimental protocol, the rate of exocytosis is generally well described by a sigmoidal function of the Ca^{2+} concentration, which is believed to reflect the intrinsic, biochemical, cooperativity of the exocytotic machinery. We can write the results of such flash-release experiments as

$$R_c = \sigma(Ca_c). \tag{5}$$

Typical half-max (K_D) parameters are of the order of tens of μM [36–38].

This relation has been (erroneously) applied (also by us [8]) to the local control of exocytosis to model whole-cell exocytosis under conditions when Ca_c is not uniform as

$$\tilde{R}_c = \sigma(\overline{Ca}_{md}) = \sigma(m^n h\, Ca_{md}). \tag{6}$$

However, the local control of exocytosis reflects the intrinsic Ca^{2+} dependence, i.e., single-microdomain exocytosis is

$$R_{md} = \sigma(Ca_{md})/n_{Ca}, \tag{7}$$

and hence whole-cell release (assuming only release from microdomains with an open channel) is

$$R_c = n_{Ca} m^n h\ R_{md} = m^n h\, \sigma(Ca_{md}). \tag{8}$$

Whereas Eq. 6 express whole-cell exocytosis as a function of average microdomain Ca^{2+}, Eq. 8 express whole-cell exocytosis as the sum of microdomain exocytosis. Because of the nonlinear, sigmoidal form of σ, R_c and $\tilde{R}_c$ differ. For example, when few channels are open, $\overline{Ca}_{md}$ may be only modestly above the bulk Ca^{2+} concentration and well below the K_D of σ, implying $\tilde{R}_c \approx 0$ suggesting almost no exocytosis. In contrast, the more correct interpretation would be the following. If the microdomain Ca^{2+} levels near open Ca^{2+} channels is well above the K_D of σ, then exocytosis would occur rapidly near these open channels, and whole-cell exocytosis could be non negligible. These arguments are summarized in Fig. 3.

In summary, since some Ca^{2+} channels are open while others are closed during electrical activity or voltage-clamp depolarizations, the Ca^{2+} level near releasable granules is nonuniform, and because of the nonlinear behavior of the exocytotic machinery whole-cell exocytosis can not be modeled as a function of the average microdomain Ca^{2+} concentrations or the bulk cytosolic Ca^{2+} level.

6.1. Distinguishing pool depletion from Ca^{2+} channel inactivation

Another widely-used electrophysiological method to study whole-cell exocytosis is to depolarize the cell membrane using voltage clamp and the patch-clamp technique [35]. The depolarization opens Ca^{2+} channels, allowing Ca^{2+} influx and exocytosis. During the depolarization it is possible to measure the Ca^{2+} current, whereas the cell capacitance C_m can only be measured reliably before and after, but not during, the depolarization. To investigate the dynamics of
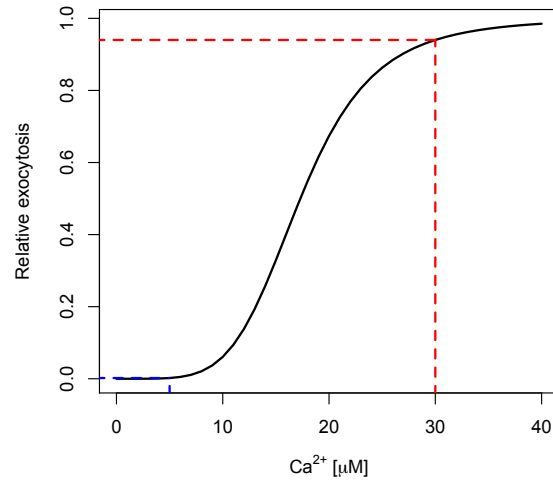
14

Figure 3: Relation between Ca^{2+} concentration and exocytosis. The curve corresponds to the sigmoidal relation between Ca^{2+} levels and exocytosis in β-cells, which can be described by a Hill function with $K_D = 17.3$ μM and Hill coefficient $n = 5$ [38]. The red dashed lines show the relative amount of exocytosis that can be expected from granules located in Ca^{2+} microdomains and exposed to 30 μM Ca^{2+}. These granules will exocytose with rate equal to 94% of their maximal rate. If for example $1/6$ of the Ca^{2+} channels are open, this would give a whole-cell exocytosis rate R_c of $\sim$16% of the maximal rate (cf. Eq. 8). If in contrast the average microdomain Ca^{2+} contration of $1/6 \cdot 30$ μM $= 5$ μM was used to calculate whole-cell exocytosis using Eq. 6, one finds that exocytosis is virtually absent ($\tilde{R}_c = 0.2\%$ of maximal whole-cell exocytosis, blue dashed curves).

exocytosis, measured as the increase in capacitance ΔC_m, it is therefore necessary to apply depolarizing pulses of varying duration. Exocytosis typically proceeds at a higher average rate during shorter than during longer depolar-
izations, which has traditionally been interpreted as being the result of the depletion of a small pool of granules located near Ca^{2+} channels, the so-called immediately releasable pool (IRP) [68].

However, the Ca^{2+} currents inactivate on a timescale similar to the decay in the rate of exocytosis. Thus, it may be that exocytosis proceeds more slowly
not because of pool depletion, but rather because the triggering Ca^{2+} signal is reduced towards the end of longer depolarizations as result of Ca^{2+} current inactivation. It has therefore been suggested that the amount of exocytosis (ΔC_m) should be related to the total amount of Ca^{2+} that entered the cell during the depolarization Q [69, 70]. For a depolarization of duration t this
quantity is described by the integral of (the absolute value of) the whole cell Ca^{2+}-current I_{Ca}, i.e., $Q(t) = \int_0^t |I_{Ca}|(s)ds$.

Recently, we investigated theoretically the interaction between pool depletion and Ca^{2+} current inactivation in details [70]. Assuming a single pool of granules that does not refill on the short time-scales relevant for the depolariza-
tion protocols, it can be shown that pool depletion can be revealed by relating the amount of exocytosis (ΔC_m) to Ca^{2+} entry (Q) as follows.

The pool size X is described by

$$\frac{dX}{dt} = -R_c(t)X, \qquad X(0) = X_0, \tag{9}$$

where $R_c(t)$ is the whole-cell rate of exocytosis, which depends on the time-varying Ca^{2+} currents, but is assumed not to depend on $X(t)$. Since refilling of the pool is slow [71–74], it is assumed not to take place during the short
(<1 second) depolarizations studied here.

The cumulative capacitance increase during a depolarization ΔC_m reflects the amount of exocytosis and is given by

$$\Delta C_m(t) = X_0 - X(t), \tag{10}$$

since no refilling is assumed. It is also assumed that endocytosis is negligible [75, 76].

Equation 9 describing the granule pool dynamics can be solved explicitly to yield

$$X(t) = X_0 \exp\left(-\int_0^t R_c(u)du\right). \tag{11}$$

When inserting this expression in Eq. 10, the following explicit formula for the cumulative capacitance is obtained,

$$\Delta C_m(t) = X_0\left(1 - \exp\left(-\int_0^t R_c(u)du\right)\right). \tag{12}$$

16

One Ca^{2+}-channel type, one channel per microdomain

When granules are located in Ca^{2+}-microdomains at the inner mouth of Ca^{2+}-channels, the rate of exocytosis is controlled by the microdomain (MD) Ca^{2+}-concentration, Ca_{md}^{2+}. Assume that all Ca^{2+}-channels are identical and spatially discrete. Then Ca_{md}^{2+} below an open Ca^{2+}-channel is approximately proportional to the single-channel current i_{Ca} [52, 77]. During voltage-clamp depolarizations, the whole-cell Ca^{2+}-current I_{Ca} might inactivate, which is caused by the closure of single Ca^{2+}-channels, i.e, the number of open channels decrease during the depolarization but with no change to the single-channel current i_{Ca} through the remaining open channels. As discusses above, this implies that the number of MDs $N_{md}(t) = n_{Ca}m^n h$, which is proportional to $I_{Ca}(t)$, decreases, but the Ca^{2+}-concentration is unchanged in the remaining MDs. The rate of exocytosis from each MD, $R_{md} = R_{md}(Ca_{md}^{2+})$, is therefore constant until the collapse of the MD because of closure of the corresponding Ca^{2+}-channel, independently of the functional form of the relation between Ca_{md}^{2+} and R_{md}. The total rate of exocytosis can then be expressed as (see Eq. 8)

$$E(t) = R_{md}N_{md}(t) = R_{md}I_{Ca}(t)/i_{Ca} = A \cdot |I_{Ca}|(t), \tag{13}$$

where $A = R_{md}/|i_{Ca}|$. From Eq. 12 we then obtain

$$\Delta C_m(t) = X_0 \left[1 - \exp\left(-AQ(t) \right) \right]. \tag{14}$$

Note that Eq. 14 describes simple first-order pool kinetics when time is rescaled to $Q(t)$.

If $AQ(t)$ is small, i.e., if the cumulative exocytotic rate is sufficiently low, then the granule pool does not deplete substantially and Eq. 14 simplifies to

$$\Delta C_m(t) = R_0 A Q(t). \tag{15}$$

Thus, in the case of no pool depletion and with exocytosis of each granule controlled by a single channel, cumulative exocytosis is linearly related to total Ca^{2+} entry [78]. However, if the granule pool is eventually depleted, then ΔC_m will be a concave function of Q (Fig. 4). Hence, ΔC_m must be analyzed as a function of Q to decide whether pool depletion occurs, since Ca^{2+}-channel inactivation might masquerade as pool depletion when considering capacitance increase as a function of depolarization length. Similar considerations and conclusions are reached also for more complex scenarios with, e.g., more Ca^{2+} channels per granule, different Ca^{2+} channel types, etc., as discusses in the original paper [70].

6.2. Mixed-effects modeling of pulse-length capacitance data

We have applied the theory from the previous section to data from pancreatic α-cells [79] and β-cells [13, 59] to investigate whether previous interpretations of depolarization-evoked exocytosis are supported when Ca^{2+} current inactivation is taken into account. We applied linear mixed-effects modeling to handle
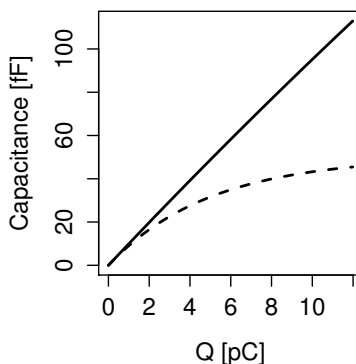
17

Figure 4: Predicted relation between Ca^{2+} influx Q and exocytosis ΔC_m in the presence (dashed curve) or absence (solid curve) of pool depletion.

cell-to-cell heterogeneity and the fact that data was obtained by applying depolarizations of different lengths to each cell, creating clustered data (Section 2.3).

We found no evidence of pool depletion in mouse α-cells [79] and β-cells [13] since the capacitance increases (reflecting exocytosis) were linearly related to Ca^{2+} influx Q. There was substantial cell-to-cell variation, highlighting the need for correcting for the clustered structure of the data. In contrast, INS-1 β-cells possess a tiny immediately releasable pool, but most exocytosis occurs proportionally to Ca^{2+} influx, suggesting that also in these cells pool depletion plays little role if shaping the exocytosis patterns seen on short, sub-second, time-scales under the conditions used in these patch-clamp experiments. We note that in other endocrine cell types there is evidence of pool depletion also when relating exocytosis to Ca^{2+} entry [71, 80]. Further, pool depletion may be important for shaping insulin secretion under more physiological settings [5, 81, 82].

7. Control of exocytosis by different types of Ca^{2+} channels

So far, we have made no distinction between how different types of Ca^{2+} channels couple to exocytosis. Since the various types of Ca^{2+} channels differ in their kinetics and single-channel currents, the relation between ΔC_m and Q can be modified considerably if exocytosis (ΔC_m) is controlled by a specific Ca^{2+} channel type while Q measure total Ca^{2+} influx through all channel types [70].

It has been suggested that in pancreatic α-cells (which release glucagon that raise the plasma glucose concentration, i.e., has the opposite effect of insulin) exocytosis is coupled to different types of Ca^{2+} channels in a complex manner controlled by cAMP, and that this arrangement underlies the fact that glucagon-like peptide 1 (GLP-1) lowers glucagon release, while adrenaline increases secretion [83], although both GLP-1 and adrenaline act via cAMP. In particular, fusion of glucagon-containing granules have been found to depend on P/Q-type Ca^{2+} channels [84]. GLP-1 raises cAMP modestly, which inhibits
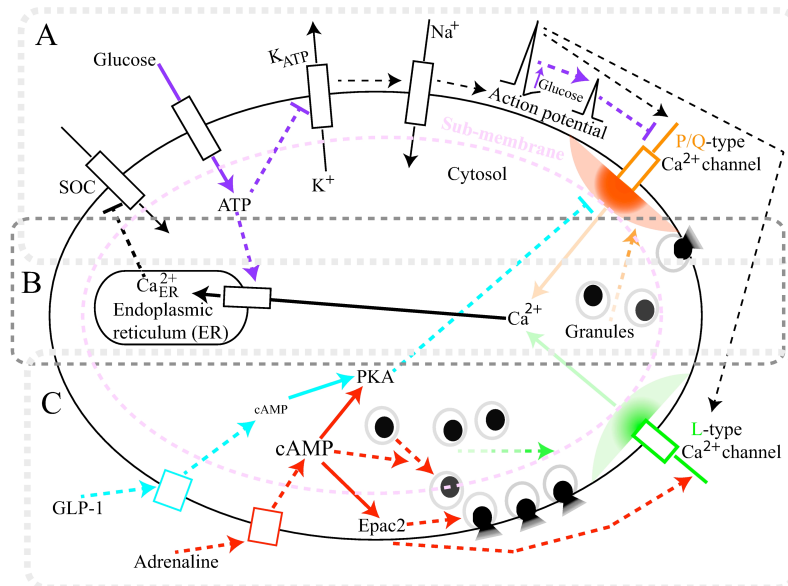
18

Figure 5: Overview of the main mechanisms underlying glucagon secretion from α-cells in response to glucose and hormones considered in the model [85]. Box A: Ion channels determining α-cell electrical activity. Box B: Ca^{2+} influx through P/Q- and L-type Ca^{2+} channels involved in exocytosis, Ca^{2+} diffusion and Ca^{2+} uptake from endoplasmic reticulum. Box C: Inhibition of glucagon secretion by GLP-1 and stimulation of release by adrenaline.

P/Q-type channels and reduces exocytosis, whereas adrenaline increases cAMP levels much more which activates L-type Ca^{2+} channels and switches exocytosis to depend on L-type Ca^{2+} currents rather than P/Q-type channels [83, 84].

Recently, we [85] devised a model that characterizes in detail ion channels, the intracellular calcium dynamics and possible priming or recruitment of granules around the Ca^{2+} channels of various types, with the aim to investigate theoretically these aspects of pancreatic α-cell function (Fig. 5). The devised mathematical model of electrical activity and exocytosis in mouse α-cells was an updated version of previous models [86, 87]. Although α-cell electrical activity is well studied [86–88], coupling to exocytosis is not. Therefore, our model coupled electrical activity to exocytosis to give a unified picture of the main mechanisms that control glucagon secretion. We modelled exocytosis as depending on the Ca^{2+} concentrations in the microdomains surrounding P/Q- and L-type Ca^{2+} channels, and the submembrane Ca^{2+} concentration.

The model [85] is able to reproduce the inhibitory effect of glucose increase on electrical activity, characterized by spikes with reduced amplitude [89]. The decrease of spike amplitude determines a significant reduction in glucagon secretion, in particular, the P/Q-type Ca^{2+} channel-dependent secretion is significantly reduced because few P/Q-type Ca^{2+} channels activate, whereas there is little variation in simulated microdomain Ca^{2+} levels [85]. Thus, it is the reduc-

19

tion in the number of open P/Q-type Ca^{2+} channels, rather than a changes in local Ca^{2+} concentration or in cytosolic Ca^{2+} levels, that underlies the inhibition of glucagon release by glucose in the model. Notably, bulk cytosolic Ca^{2+} levels increased in our simulation. Similarly, when we simulated the inhibitory effect of GLP-1 on P/Q-type Ca^{2+} channels, glucagon secretion was reduced because of closing of the P/Q-type channels, and not because of a reduction in local or global Ca^{2+} concentrations [85].

The model was also able to reproduce the effect of adrenaline at low (1 mM) and at physiological (6 mM) glucose levels. The adrenaline effect is simulated by increasing the L-type Ca^{2+} channel conductance, and decreasing the threshold value for exocytosis near L-type Ca^{2+} channels, in order to model the cAMP-mediated increase of the L-type Ca^{2+} currents, and possible priming or recruitment of granules around the L-type Ca^{2+} channels [83, 90]. Moreover, we included the antagonistic effect of cAMP on P/Q-type Ca^{2+} channels, as for the GLP-1 simulation. At both glucose levels, in response to adrenaline, the simulated electrical activity exhibits reduced spike amplitude with an additional decrease at the higher glucose level. The L-type Ca^{2+} channels mainly determine the glucagon secretion increase due to adrenaline: the microdomain Ca^{2+} concentration surrounding the open L-type Ca^{2+} channels increases at both glucose levels and is much higher than the threshold value for exocytosis. This effect compensates for the small decrease in the open probability for the L-type Ca^{2+} channels. The P/Q-type Ca^{2+} channel-dependent secretion is significantly reduced, as for the simulated GLP-1 effect, while the intracellular Ca^{2+} concentration shows a small increase. Thus, in our model [85], adrenaline can effectively shift exocytosis from P/Q-type to L-type Ca^{2+} channels, as has been suggested previously [83, 91].

For the simulated effects produced by glucose increase and adrenaline, the model showed a rise of the bulk cytosolic Ca^{2+} levels during the simulated effects. However, only for adrenaline was an increase of glucagon secretion correlated with a rise in global Ca^{2+}. Interestingly, bulk α-cell Ca^{2+} levels in response to elevations in glucose concentrations have been reported to increase [91, 92], remain unchanged [93, 94], or even decrease [95, 96]. Hence, whole-cell Ca^{2+} concentrations does not necessarily reflect glucagon secretion, as shown by our simulations. In particular, our model highlights how glucose uncouples the positive relationship between the cytosolic Ca^{2+} concentration and secretory activity [92] because of control of exocytosis by Ca^{2+} microdomains and mechanisms downstream of electrical activity.

8. Conclusions

In this review we provided an overview of recent quantitative approaches to the study of exocytosis with focus on local control of exocytosis by Ca^{2+} microdomains. Reflecting our current personal interests, we have limited the discussion mostly to endocrine cells, and only briefly treated models of dynamics between different pools of granules.

An important aspect presented here is that whole-cell models should be consistent with the mechanisms operating on lower biological scales, as discussed in Section 6. This approach is needed to investigate thoroughly how glucagon secretion can 'decouple' from global Ca^{2+} levels, as shown in Section 7. Although local Ca^{2+} elevation due to buffered diffusion can be simulated and provide important insight into local control of exocytosis (Sections 4 and 5), we advocate that simplifications considering microdomains as compartments give important insight at the whole-cell level. In other words, the model should be chosen according to the purpose.

We have given examples of two kinds of mathematical models. One is used to get insight into a particular experiment. This was for example the case for our diffusion model, which was developed to understand better the TIRF data (Section 4). In particular, the model highlighted that the Ca^{2+}-sensor signal saturated, and hence that the amplitude of the signal did not give much information. In contrast, the risetime of the signal showed a robust relation to the distance to a Ca^{2+} channel. Another example of such experiment-specific modeling was the investigation of the relation between capacitance increases and Ca^{2+} influx in the pulse-length protocol (Section 6.1 and [70]). Because of the close relation to experimental data, these models are advantageously combined with advanced statistical methods, such as time-to-event analysis (Section 4) and mixed-effects modeling (Section 6.2) in order to perform powerful and statistically sound inference.

The other type of model is used to simulate 'what-if' scenarios. For example, we have investigated how different electrical patterns control exocytosis in pituitary cells (Section 5 and [67]). We also investigated if the biological hypotheses concerning differential control of exocytosis by different types of Ca^{2+} channels in α-cells were consistent with data, and could simulate e.g. the mechanisms of adrenaline-stimulated glucagon secretion at various glucose levels (Section 7 and [85]).

In summary, mathematical and statistical modeling can and should be used to maximize the information that can be extracted from exoytosis data, to investigate specific biological hypotheses, and to predict the answer to 'what-if' questions, thus suggesting new experiments.

References

[1] S. Misler, Unifying concepts in stimulus-secretion coupling in endocrine cells and some implications for therapeutics., Adv Physiol Educ 33 (3) (2009) 175–186. doi:10.1152/advan.90213.2008.
URL http://dx.doi.org/10.1152/advan.90213.2008

[2] F. M. Ashcroft, P. Rorsman, Diabetes mellitus and the β cell: the last ten years, Cell 148 (6) (2012) 1160–71. doi:10.1016/j.cell.2012.02.010.

[3] S. Barg, Mechanisms of exocytosis in insulin-secreting B-cells and glucagon-secreting A-cells., Pharmacol Toxicol 92 (1) (2003) 3–13.

[4] R. D. Burgoyne, A. Morgan, Secretory granule exocytosis., Physiol Rev
83 (2) (2003) 581–632. `doi:10.1152/physrev.00031.2002`.
URL `http://dx.doi.org/10.1152/physrev.00031.2002`

[5] G. M. Grodsky, A threshold distribution hypothesis for packet storage of
insulin and its mathematical modeling., J. Clin. Invest. 51 (1972) 2047–
2059. `doi:10.1172/JCI107011`.
URL `http://dx.doi.org/10.1172/JCI107011`

[6] T. Voets, Dissection of three Ca2+-dependent steps leading to secretion in
chromaffin cells from mouse adrenal slices., Neuron 28 (2) (2000) 537–545.

[7] P. Rorsman, E. Renström, Insulin granule dynamics in pancreatic
beta cells., Diabetologia 46 (8) (2003) 1029–1045. `doi:10.1007/`
`s00125-003-1153-1`.
URL `http://dx.doi.org/10.1007/s00125-003-1153-1`

[8] M. G. Pedersen, A. Sherman, Newcomer insulin secretory granules as a
highly calcium-sensitive pool., Proc Natl Acad Sci U S A 106 (18) (2009)
7432–7436. `doi:10.1073/pnas.0901202106`.
URL `http://dx.doi.org/10.1073/pnas.0901202106`

[9] E. Neher, Merits and limitations of vesicle pool models in view of hetero-
geneous populations of synaptic vesicles, Neuron 87 (6) (2015) 1131–42.
`doi:10.1016/j.neuron.2015.08.038`.

[10] S. Barg, P. Huang, L. Eliasson, D. J. Nelson, S. Obermüller, P. Rorsman,
F. Thévenod, E. Renström, Priming of insulin granules for exocytosis by
granular Cl(-) uptake and acidification, J Cell Sci 114 (Pt 11) (2001) 2145–
54.

[11] N. R. Gandasi, S. Barg, Contact-induced clustering of syntaxin and munc18
docks secretory granules at the exocytosis site, Nat Commun 5 (2014) 3914.
`doi:10.1038/ncomms4914`.

[12] E. Neher, T. Sakaba, Multiple roles of calcium ions in the regulation of
neurotransmitter release., Neuron 59 (6) (2008) 861–872. `doi:10.1016/j.`
`neuron.2008.08.019`.
URL `http://dx.doi.org/10.1016/j.neuron.2008.08.019`

[13] M. G. Pedersen, G. Cortese, L. Eliasson, Mathematical modeling and sta-
tistical analysis of calcium-regulated insulin granule exocytosis in β-cells
from mice and humans, Prog Biophys Mol Biol 107 (2) (2011) 257–64.
`doi:10.1016/j.pbiomolbio.2011.07.012`.
URL `http://dx.doi.org/10.1016/j.pbiomolbio.2011.07.012`

[14] P. Palumbo, S. Ditlevsen, A. Bertuzzi, A. De Gaetano, Mathematical mod-
eling of the glucose-insulin system: a review, Math Biosci 244 (2) (2013)
69–81. `doi:10.1016/j.mbs.2013.05.006`.

[15] E. Neher, A. Marty, Discrete changes of cell membrane capacitance observed under conditions of enhanced secretion in bovine adrenal chromaffin cells., Proc Natl Acad Sci U S A 79 (21) (1982) 6712–6716.

[16] W. Almers, E. Neher, Gradual and stepwise changes in the membrane capacitance of rat peritoneal mast cells, J Physiol 386 (1987) 205–17.

[17] G. Dernick, G. Alvarez de Toledo, M. Lindau, Exocytosis of single chromaffin granules in cell-free inside-out membrane patches, Nat Cell Biol 5 (4) (2003) 358–62. doi:10.1038/ncb956.

[18] P. E. MacDonald, S. Obermüller, J. Vikman, J. Galvanovskis, P. Rorsman, L. Eliasson, Regulated exocytosis and kiss-and-run of synaptic-like microvesicles in ins-1 and primary rat beta-cells, Diabetes 54 (3) (2005) 736–43.

[19] N. Takahashi, T. Kishimoto, T. Nemoto, T. Kadowaki, H. Kasai, Fusion pore dynamics and insulin granule exocytosis in the pancreatic islet, Science 297 (5585) (2002) 1349–52. doi:10.1126/science.1073806.

[20] S. Obermüller, F. Calegari, A. King, A. Lindqvist, I. Lundquist, A. Salehi, M. Francolini, P. Rosa, P. Rorsman, W. B. Huttner, S. Barg, Defective secretion of islet hormones in chromogranin-b deficient mice, PLoS One 5 (1) (2010) e8936. doi:10.1371/journal.pone.0008936.

[21] J. T. Low, J. M. Mitchell, O. H. Do, J. Bax, A. Rawlings, M. Zavortink, G. Morgan, R. G. Parton, H. Y. Gaisano, P. Thorn, Glucose principally regulates insulin secretion in mouse islets by controlling the numbers of granule fusion events per cell, Diabetologiadoi:10.1007/s00125-013-3019-5.

[22] D. J. Michael, X. Geng, N. X. Cawley, Y. P. Loh, C. J. Rhodes, P. Drain, R. H. Chow, Fluorescent cargo proteins in pancreatic beta-cells: design determines secretion kinetics at exocytosis, Biophys J 87 (6) (2004) L03–5. doi:10.1529/biophysj.104.052175.

[23] N. R. Gandasi, K. Vestö, M. Helou, P. Yin, J. Saras, S. Barg, Survey of red fluorescence proteins as markers for secretory granule exocytosis, PLoS One 10 (6) (2015) e0127801. doi:10.1371/journal.pone.0127801.

[24] T. Lang, I. Wacker, J. Steyer, C. Kaether, I. Wunderlich, T. Soldati, H. H. Gerdes, W. Almers, Ca2+-triggered peptide secretion in single cells imaged with green fluorescent protein and evanescent-wave microscopy, Neuron 18 (6) (1997) 857–63.

[25] J. A. Steyer, H. Horstmann, W. Almers, Transport, docking and exocytosis of single secretory granules in live chromaffin cells, Nature 388 (6641) (1997) 474–8. doi:10.1038/41329.

[26] M. Oheim, D. Loerke, W. Stühmer, R. H. Chow, The last few milliseconds in the life of a secretory granule. docking, dynamics and fusion visualized by total internal reflection fluorescence microscopy (tirfm), Eur Biophys J 27 (2) (1998) 83–98.

[27] M. Ohara-Imaizumi, Y. Nakamichi, T. Tanaka, H. Ishida, S. Nagamatsu, Imaging exocytosis of single insulin secretory granules with evanescent wave microscopy: distinct behavior of granule motion in biphasic insulin release, J Biol Chem 277 (6) (2002) 3805–8. doi:10.1074/jbc.C100712200.

[28] D. J. Michael, W. Xiong, X. Geng, P. Drain, R. H. Chow, Human insulin vesicle dynamics during pulsatile secretion, Diabetes 56 (5) (2007) 1277–88. doi:10.2337/db06-0367.

[29] S. Barg, M. K. Knowles, X. Chen, M. Midorikawa, W. Almers, Syntaxin clusters assemble reversibly at sites of secretory granules in live cells, Proc Natl Acad Sci U S A 107 (48) (2010) 20804–9. doi:10.1073/pnas.1014823107.

[30] D. Toomre, Generating live cell data using total internal reflection fluorescence microscopy, Cold Spring Harb Protoc 2012 (4) (2012) 439–46. doi:10.1101/pdb.ip068676.

[31] M. Midorikawa, T. Sakaba, Imaging exocytosis of single synaptic vesicles at a fast CNS presynaptic terminal, Neuron 88 (3) (2015) 492–8. doi:10.1016/j.neuron.2015.09.047.

[32] U. Becherer, T. Moser, W. Stühmer, M. Oheim, Calcium regulates exocytosis at the level of single vesicles, Nat Neurosci 6 (8) (2003) 846–53. doi:10.1038/nn1087.

[33] M. B. Hoppa, S. Collins, R. Ramracheya, L. Hodson, S. Amisten, Q. Zhang, P. Johnson, F. M. Ashcroft, P. Rorsman, Chronic palmitate exposure inhibits insulin secretion by dissociation of Ca(2+) channels from secretory granules, Cell Metab 10 (6) (2009) 455–65. doi:10.1016/j.cmet.2009.09.011.

[34] A. J. Trexler, K. A. Sochacki, J. W. Taraska, Imaging the recruitment and loss of proteins and lipids at single sites of calcium-triggered exocytosis, Mol Biol Cell 27 (15) (2016) 2423–34. doi:10.1091/mbc.E16-01-0057.

[35] M. Lindau, E. Neher, Patch-clamp techniques for time-resolved capacitance measurements in single cells., Pflugers Arch 411 (2) (1988) 137–146.

[36] P. Thomas, J. G. Wong, A. K. Lee, W. Almers, A low affinity Ca2+ receptor controls the final steps in peptide secretion from pituitary melanotrophs., Neuron 11 (1) (1993) 93–104.

[37] C. Heinemann, R. H. Chow, E. Neher, R. S. Zucker, Kinetics of the secretory response in bovine chromaffin cells following flash photolysis of caged Ca2+., Biophys J 67 (6) (1994) 2546–2557. `doi:10.1016/S0006-3495(94)80744-1`.
URL `http://dx.doi.org/10.1016/S0006-3495(94)80744-1`

[38] S. Barg, X. Ma, L. Eliasson, J. Galvanovskis, S. O. Göpel, S. Obermüller, J. Platzer, E. Renström, M. Trus, D. Atlas, J. Striessnig, P. Rorsman, Fast exocytosis with few Ca(2+) channels in insulin-secreting mouse pancreatic B cells., Biophys J 81 (6) (2001) 3308–3323.

[39] Y. Yang, S. Udayasankar, J. Dunning, P. Chen, K. D. Gillis, A highly ca2+-sensitive pool of vesicles is regulated by protein kinase c in adrenal chromaffin cells., Proc Natl Acad Sci U S A 99 (26) (2002) 17060–17065. `doi:10.1073/pnas.242624699`.
URL `http://dx.doi.org/10.1073/pnas.242624699`

[40] Y. Yang, K. D. Gillis, A highly Ca2+-sensitive pool of granules is regulated by glucose and protein kinases in insulin-secreting INS-1 cells., J Gen Physiol 124 (6) (2004) 641–651. `doi:10.1085/jgp.200409081`.
URL `http://dx.doi.org/10.1085/jgp.200409081`

[41] Q.-F. Wan, Y. Dong, H. Yang, X. Lou, J. Ding, T. Xu, Protein kinase activation increases insulin secretion by sensitizing the secretory machinery to Ca2+., J Gen Physiol 124 (6) (2004) 653–662. `doi:10.1085/jgp.200409082`.
URL `http://dx.doi.org/10.1085/jgp.200409082`

[42] A. M. Walter, P. S. Pinheiro, M. Verhage, J. B. Sørensen, A sequential vesicle pool model with a single release sensor and a ca(2+)-dependent priming catalyst effectively explains ca(2+)-dependent properties of neurosecretion, PLoS Comput Biol 9 (12) (2013) e1003362. `doi:10.1371/journal.pcbi.1003362`.

[43] W. N. Venables, B. D. Ripley, Modern Applied Statistics with S, 4th Edition, Springer, New York, 2002.

[44] R. E. Chandler, S. Bate, Inference for clustered data using the independence loglikelihood, Biometrika 94 (1) (2007) 167–183.

[45] J. C. Pinheiro, D. M. Bates, Mixed-Effects Models in S and S-PLUS, Springer, New York, 2000.

[46] B. Katz, R. Miledi, The effect of calcium on acetylcholine release from motor nerve terminals, Proc R Soc Lond B Biol Sci 161 (1965) 496–503.

[47] W. W. Douglas, R. P. Rubin, The role of calcium in the secretory response of the adrenal medulla to acetylcholine, J Physiol 159 (1961) 40–57.

[48] W. W. Douglas, Stimulus-secretion coupling: the concept and clues from chromaffin and other cells, Br J Pharmacol 34 (3) (1968) 451–74.

[49] R. Schneggenburger, Y. Han, O. Kochubey, Ca(2+) channels and transmitter release at the active zone, Cell Calcium 52 (3-4) (2012) 199–207. `doi:10.1016/j.ceca.2012.04.011`.

[50] J. E. Chad, R. Eckert, Calcium domains associated with individual channels can account for anomalous voltage relations of CA-dependent responses, Biophys J 45 (5) (1984) 993–9. `doi:10.1016/S0006-3495(84)84244-7`.

[51] S. M. Simon, R. R. Llinás, Compartmentalization of the submembrane calcium activity during calcium influx and its significance in transmitter release., Biophys J 48 (3) (1985) 485–498. `doi:10.1016/S0006-3495(85)83804-2`.
URL `http://dx.doi.org/10.1016/S0006-3495(85)83804-2`

[52] E. Neher, Vesicle pools and Ca2+ microdomains: new tools for understanding their roles in neurotransmitter release., Neuron 20 (3) (1998) 389–399.

[53] E. Neher, Usefulness and limitations of linear approximations to the understanding of Ca++ signals, Cell Calcium 24 (5-6) (1998) 345–57.

[54] J. Klingauf, E. Neher, Modeling buffered Ca2+ diffusion near the membrane: implications for secretion in neuroendocrine cells., Biophys J 72 (2 Pt 1) (1997) 674–690.

[55] K. S. Kits, T. A. de Vlieger, B. W. Kooi, H. D. Mansvelder, Diffusion barriers limit the effect of mobile calcium buffers on exocytosis of large dense cored vesicles., Biophys J 76 (3) (1999) 1693–1705. `doi:10.1016/S0006-3495(99)77328-5`.
URL `http://dx.doi.org/10.1016/S0006-3495(99)77328-5`

[56] V. Shahrezaei, K. R. Delaney, Consequences of molecular-level Ca2+ channel and synaptic vesicle colocalization for the Ca2+ microdomain and neurotransmitter exocytosis: a monte carlo study, Biophys J 87 (4) (2004) 2352–64. `doi:10.1529/biophysj.104.043380`.

[57] L. Catacuzzeno, B. Fioretti, F. Franciolini, Modeling study of the effects of membrane surface charge on calcium microdomains and neurotransmitter release, Biophys J 95 (5) (2008) 2160–71. `doi:10.1529/biophysj.107.124909`.

[58] V. Matveev, R. S. Zucker, A. Sherman, Facilitation through buffer saturation: constraints on endogenous buffering properties., Biophys J 86 (5) (2004) 2691–2709. `doi:10.1016/S0006-3495(04)74324-6`.
URL `http://dx.doi.org/10.1016/S0006-3495(04)74324-6`

[59] M. G. Pedersen, V. A. Salunkhe, E. Svedin, A. Edlund, L. Eliasson, Calcium current inactivation rather than pool depletion explains reduced exocytotic rate with prolonged stimulation in insulin-secreting ins-1 832/13 cells, PLoS One 9 (8) (2014) e103874. `doi:10.1371/journal.pone.0103874`.

[60] J. P. Klein, M. L. Moeschberger, Survival analysis: techniques for censored and truncated data, Springer Science & Business Media, 2005.

[61] G. Cortese, T. H. Scheike, T. Martinussen, Flexible survival regression modelling, Stat Methods Med Res 19 (1) (2010) 5–28. `doi:10.1177/0962280209105022`.

[62] W. Q. Meeker, L. A. Escobar, Statistical methods for reliability data, John Wiley & Sons, 2014.

[63] A. Wienke, Frailty models in survival analysis, CRC Press, 2010.

[64] F. Van Goor, D. Zivadinovic, A. J. Martinez-Fuentes, S. S. Stojilkovic, Dependence of pituitary hormone secretion on the pattern of spontaneous voltage-gated calcium influx. cell type-specific action potential secretion coupling, J Biol Chem 276 (36) (2001) 33840–6. `doi:10.1074/jbc.M105386200`.

[65] S. S. Stojilkovic, H. Zemkova, F. Van Goor, Biophysical basis of pituitary cell type-specific ca2+ signaling-secretion coupling, Trends Endocrinol Metab 16 (4) (2005) 152–9. `doi:10.1016/j.tem.2005.03.003`.

[66] J. Tabak, M. Tomaiuolo, A. E. Gonzalez-Iglesias, L. S. Milescu, R. Bertram, Fast-activating voltage- and calcium-dependent potassium (BK) conductance promotes bursting in pituitary cells: a dynamic clamp study, J Neurosci 31 (46) (2011) 16855–63. `doi:10.1523/JNEUROSCI.3235-11.2011`.

[67] A. Tagliavini, J. Tabak, R. Bertram, M. G. Pedersen, Is bursting more effective than spiking in evoking pituitary hormone secretion? a spatiotemporal simulation study of calcium and granule dynamics, Am J Physiol Endocrinol Metab 310 (7) (2016) E515–25. `doi:10.1152/ajpendo.00500.2015`.

[68] F. T. Horrigan, R. J. Bookman, Releasable pools and the kinetics of exocytosis in adrenal chromaffin cells., Neuron 13 (5) (1994) 1119–1129.

[69] K. L. Engisch, M. C. Nowycky, Calcium dependence of large dense-cored vesicle exocytosis evoked by calcium influx in bovine adrenal chromaffin cells., J Neurosci 16 (4) (1996) 1359–1369.

[70] M. G. Pedersen, On depolarization-evoked exocytosis as a function of calcium entry: possibilities and pitfalls, Biophys J 101 (4) (2011) 793–802. `doi:10.1016/j.bpj.2011.06.061`.

[71] T. Moser, E. Neher, Rapid exocytosis in single chromaffin cells recorded from mouse adrenal slices., J Neurosci 17 (7) (1997) 2314–2323.

[72] J. Gromada, M. Høy, E. Renström, K. Bokvist, L. Eliasson, S. Göpel, P. Rorsman, Cam kinase ii-dependent mobilization of secretory granules underlies acetylcholine-induced stimulation of exocytosis in mouse pancreatic b-cells., J Physiol 518 (Pt 3) (1999) 745–759.

[73] T. Voets, E. Neher, T. Moser, Mechanisms underlying phasic and sustained secretion in chromaffin cells from mouse adrenal slices., Neuron 23 (3) (1999) 607–615.

[74] T. Rose, S. Efendic, M. Rupnik, Ca2+-secretion coupling is impaired in diabetic Goto Kakizaki rats., J Gen Physiol 129 (6) (2007) 493–508. doi: 10.1085/jgp.200609604.
URL http://dx.doi.org/10.1085/jgp.200609604

[75] L. Eliasson, P. Proks, C. Ammälä, F. M. Ashcroft, K. Bokvist, E. Renström, P. Rorsman, P. A. Smith, Endocytosis of secretory granules in mouse pancreatic beta-cells evoked by transient elevation of cytosolic calcium., J Physiol 493 (Pt 3) (1996) 755–767.

[76] C. Smith, E. Neher, Multiple forms of endocytosis in bovine adrenal chromaffin cells., J Cell Biol 139 (4) (1997) 885–894.

[77] A. Sherman, J. Keizer, J. Rinzel, Domain model for Ca2(+)-inactivation of Ca2+ channels at low channel density., Biophys J 58 (4) (1990) 985–995. doi:10.1016/S0006-3495(90)82443-7.
URL http://dx.doi.org/10.1016/S0006-3495(90)82443-7

[78] G. J. Augustine, E. M. Adler, M. P. Charlton, The calcium signal for transmitter secretion from presynaptic nerve terminals., Ann N Y Acad Sci 635 (1991) 365–381.

[79] S. A. Andersson, M. G. Pedersen, J. Vikman, L. Eliasson, Glucose-dependent docking and snare protein-mediated exocytosis in mouse pancreatic alpha-cell, Pflugers Arch 462 (3) (2011) 443–54. doi:10.1007/s00424-011-0979-5.

[80] P. Rorsman, M. Braun, Regulation of insulin secretion in human pancreatic islets, Annu Rev Physiol 75 (2013) 155–79. doi:10.1146/annurev-physiol-030212-183754.

[81] C. S. Olofsson, S. O. Göpel, S. Barg, J. Galvanovskis, X. Ma, A. Salehi, P. Rorsman, L. Eliasson, Fast insulin secretion reflects exocytosis of docked granules in mouse pancreatic B-cells., Pflugers Arch 444 (1-2) (2002) 43–51. doi:10.1007/s00424-002-0781-5.
URL http://dx.doi.org/10.1007/s00424-002-0781-5

[82] J.-C. Henquin, N. Ishiyama, M. Nenquin, M. A. Ravier, J.-C. Jonas, Signals and pools underlying biphasic insulin secretion., Diabetes 51 Suppl 1 (2002) S60–S67.

[83] Y. Z. De Marinis, A. Salehi, C. E. Ward, Q. Zhang, F. Abdulkader, M. Bengtsson, O. Braha, M. Braun, R. Ramracheya, S. Amisten, A. M. Habib, Y. Moritoh, E. Zhang, F. Reimann, A. H. Rosengren, T. Shibasaki, F. Gribble, E. Renström, S. Seino, L. Eliasson, P. Rorsman, GLP-1 inhibits and adrenaline stimulates glucagon release by differential modulation of N- and L-type Ca2+ channel-dependent exocytosis., Cell Metab 11 (6) (2010) 543–553. `doi:10.1016/j.cmet.2010.04.007`.
URL `http://dx.doi.org/10.1016/j.cmet.2010.04.007`

[84] P. Rorsman, M. Braun, Q. Zhang, Regulation of calcium in pancreatic α- and β-cells in health and disease, Cell Calcium 51 (3-4) (2012) 300–8. `doi:10.1016/j.ceca.2011.11.006`.

[85] F. Montefusco, M. G. Pedersen, Mathematical modelling of local calcium and regulated exocytosis during inhibition and stimulation of glucagon secretion from pancreatic alpha-cells, J Physiol 593 (20) (2015) 4519–30. `doi:10.1113/JP270777`.

[86] P. M. Diderichsen, S. O. Göpel, Modelling the electrical activity of pancreatic alpha-cells based on experimental data from intact mouse islets, J Biol Phys 32 (3-4) (2006) 209–29. `doi:10.1007/s10867-006-9013-0`.

[87] M. Watts, A. Sherman, Modeling the pancreatic α-cell: dual mechanisms of glucose suppression of glucagon secretion, Biophys J 106 (3) (2014) 741–51. `doi:10.1016/j.bpj.2013.11.4504`.

[88] M. G. Pedersen, I. Ahlstedt, M. F. El Hachmane, S. O. Göpel, Dapagliflozin stimulates glucagon secretion at high glucose: experiments and mathematical simulations of human a-cells, Sci Rep 6 (2016) 31214. `doi:10.1038/srep31214`.

[89] Q. Zhang, R. Ramracheya, C. Lahmann, A. Tarasov, M. Bengtsson, O. Braha, M. Braun, M. Brereton, S. Collins, J. Galvanovskis, A. Gonzalez, L. N. Groschner, N. J. G. Rorsman, A. Salehi, M. E. Travers, J. N. Walker, A. L. Gloyn, F. Gribble, P. R. V. Johnson, F. Reimann, F. M. Ashcroft, P. Rorsman, Role of KATP channels in glucose-regulated glucagon secretion and impaired counterregulation in type 2 diabetes, Cell Metab 18 (6) (2013) 871–82. `doi:10.1016/j.cmet.2013.10.014`.

[90] J. Gromada, K. Bokvist, W. G. Ding, S. Barg, K. Buschard, E. Renström, P. Rorsman, Adrenaline stimulates glucagon secretion in pancreatic A-cells by increasing the Ca2+ current and the number of granules close to the L-type Ca2+ channels, J Gen Physiol 110 (3) (1997) 217–28.

29

[91] P. Rorsman, R. Ramracheya, N. J. G. Rorsman, Q. Zhang, ATP-regulated potassium channels and voltage-gated calcium channels in pancreatic alpha and beta cells: similar functions but reciprocal effects on secretion, Diabetologia 57 (9) (2014) 1749–61. doi:10.1007/s00125-014-3279-8.

[92] S. J. Le Marchand, D. W. Piston, Glucose suppression of glucagon secretion: metabolic and calcium responses from alpha-cells in intact mouse pancreatic islets, J Biol Chem 285 (19) (2010) 14389–98. doi:10.1074/jbc.M109.069195.

[93] Y. Nakamura, J. Bryan, Targeting SUR1/Abcc8-type neuroendocrine KATP channels in pancreatic islet cells, PLoS One 9 (3) (2014) e91525. doi:10.1371/journal.pone.0091525.

[94] A. D. Elliott, A. Ustione, D. W. Piston, Somatostatin and insulin mediate glucose-inhibited glucagon secretion in the pancreatic α-cell by lowering camp, Am J Physiol Endocrinol Metab 308 (2) (2015) E130–43. doi:10.1152/ajpendo.00344.2014.

[95] P. E. MacDonald, P. Rorsman, The ins and outs of secretion from pancreatic beta-cells: control of single-vesicle exo- and endocytosis, Physiology (Bethesda) 22 (2007) 113–21. doi:10.1152/physiol.00047.2006.

[96] N. Quoix, R. Cheng-Xue, L. Mattart, Z. Zeinoun, Y. Guiot, M. C. Beauvois, J.-C. Henquin, P. Gilon, Glucose and pharmacological modulators of ATP-sensitive K+ channels control [Ca2+]c by different mechanisms in isolated mouse alpha-cells, Diabetes 58 (2) (2009) 412–21. doi:10.2337/db07-1298.